Systemic overexpression of C-C motif chemokine ligand 2 promotes metabolic dysregulation and premature death in mice with accelerated aging

Fedra Luciano-Mateo[1,2], Noemí Cabré[1,2], Gerard Baiges-Gaya[1,2], Salvador Fernández-Arroyo[1,2], Anna Hernández-Aguilera[2], Elisabet Rodríguez-Tomàs[2], Meritxell Arenas[3], Jordi Camps[1,2], Javier A. Menéndez[4,5], Jorge Joven[1,2,6]

[1]Universitat Rovira i Virgili, Department of Medicine and Surgery, Reus 43201, Spain
[2]Unitat de Recerca Biomèdica, Hospital Universitari Sant Joan, Institut d'Investigació Sanitària Pere Virgili, Universitat Rovira i Virgili, Reus 43201, Spain
[3]Department of Radiation Oncology, Hospital Universitari Sant Joan, Institut d'Investigació Sanitària Pere Virgili, Universitat Rovira i Virgili, Reus 43204, Spain
[4]Program Against Cancer Therapeutic Resistance (ProCURE), Metabolism and Cancer Group, Catalan Institute of Oncology, Girona 17007, Spain
[5]Girona Biomedical Research Institute (IDIBGI), Girona 17190, Spain
[6] The Campus of International Excellence Southern Catalonia, Tarragona 43003, Spain

Correspondence to: Jordi Camps, Jorge Joven; email: jcamps@grupsagessa.com, Jorge.joven@urv.cat

ABSTRACT

Injection of tissues with senescent cells induces changes that mimic aging, and this process is delayed in mice engineered to eliminate senescent cells, which secrete proinflammatory cytokines, including C-C motif chemokine ligand 2 (*Ccl2*). Circulating levels of *Ccl2* correlate with age, but the impact of *Ccl2* on tissue homeostasis has not been established. We generated an experimental model by crossbreeding mice overexpressing *Ccl2* with progeroid mice bearing a mutation in the lamin A (*Lmna*) gene. Wild-type animals and progeroid mice that do not overexpress *Ccl2* were used as controls. *Ccl2* overexpression decreased the lifespan of the progeroid mice and induced the dysregulation of glycolysis, the citric acid cycle and one-carbon metabolism in skeletal muscle, driving dynamic changes in energy metabolism and DNA methylation. This impact on cellular bioenergetics was associated with mitochondrial alterations and affected cellular metabolism, autophagy and protein synthesis through AMPK/mTOR pathways. The data revealed the ability of *Ccl2* to promote death in mice with accelerated aging, which supports its putative use as a biomarker of an increased senescent cell burden and for the assessment of the efficacy of interventions aimed at extending healthy aging.

INTRODUCTION

Mechanisms leading to accelerated aging are not completely understood but might converge at points of inflammation and undesirable metabolic alterations [1, 2]. Indeed, the increased incidence of chronic noncommunicable diseases during aging is closely related to the progressive decline of immune and metabolic functions. Understanding how and why we age and how to manage immunometabolic alterations

in elderly individuals are fundamental challenges to the field of medicine [2, 3]. Metformin, a drug that may potentially modulate the interplay between the metabolic processes associated with inflammation and cellular senescence, has been chosen to explore pharmacologic effects that target aging-related pathways [4–6]. Clinical trials aimed to test potential anti-aging treatments confront multiple limitations because of the extensive time between the interventions and the expected outcomes. No easily accessible biomarkers enable the prediction of functional capabilities, establishment of surrogate end-points, assessment of changes in the processes associated with aging or measurements of biological age [7–9]. A promising exception might be a multitissue DNA methylation-based age estimator applicable throughout the entire age spectrum [10, 11]. Its use in epidemiological studies indicates that epigenetic markers of aging acceleration appear to be closely associated with metabolic and inflammatory biomarkers [12]. Senescent cells in a permanent state of cycle arrest progressively accumulate during aging and contribute to the release of components associated with the senescence-associated secretory phenotype (SASP), which may partially explain the increased metabolic inflammation observed during the aging process [13–17]. These findings support the putative relevance of an abnormal secretion of proinflammatory cytokines and C-C motif chemokine ligand 2 (*Ccl2*) during aging. High levels of circulating *Ccl2* are common in diseases associated with tissue injury and have also been shown to correlate with biological age. Such associations likely reflect an increased burden of senescent cells and have been proposed as potential tools to measure the effect of interventions aimed at extending healthy aging [18, 19].

To investigate the effects of the systemic increase in *Ccl2* expression on progeria-induced metabolic derangement and lifespan, we generated an experimental model by crossbreeding mice that overexpress *Ccl2* [20] with mice bearing a mutation in exon 11 of the lamin A gene (*Lmna*) to obtain offspring that recapitulate most of the clinical features of Hutchinson-Gilford progeria syndrome in humans (HPGS) [21–23]. Histological evidence obtained from these models and the particular relevance of muscle-wasting disorders in the aging population suggest the importance of specifically exploring molecular processes associated with aging in skeletal muscle, including energy and one-carbon (1-C) metabolism alterations or mitochondrial dysfunction, and the metabolic pathways associated with cell survival [22, 23]. Our findings suggest that *Ccl2* is involved in the aging process and should be considered in the assessment of immunometabolic dysfunction in age-related diseases.

RESULTS

Ccl2 overexpression reduced the lifespan of mice with accelerated aging

The increase in body weight significantly differed among strains, and *Ccl2* overexpression was associated with different body weight changes, significant impairment in fertility, earlier-than-normal dermal thinning and considerable loss of muscle and fat. Mice with a single mutation in lamin A (LMNAG609G/+) gradually lost weight with respect to the weight of the wild-type mice from 25 to 32 weeks and the mice with a mutation in lamin A and overexpressing Ccl2 (LMNAG609G/+;CGCCL2+/-) from 12 to 14 weeks (Figure 1A). The progeroid strains also progressively diverged in terms of the development of features of accelerated aging, including growth rate, lipodystrophy and lordokyphosis (Figure 1B). The median lifespan was significantly reduced (33%) in the mice with overexpressed *Ccl2* (45 weeks for the LMNAG609G/+ mice and 30 weeks for the LMNAG609G/+;CGCCL2+/- mice) (Figure 1C).
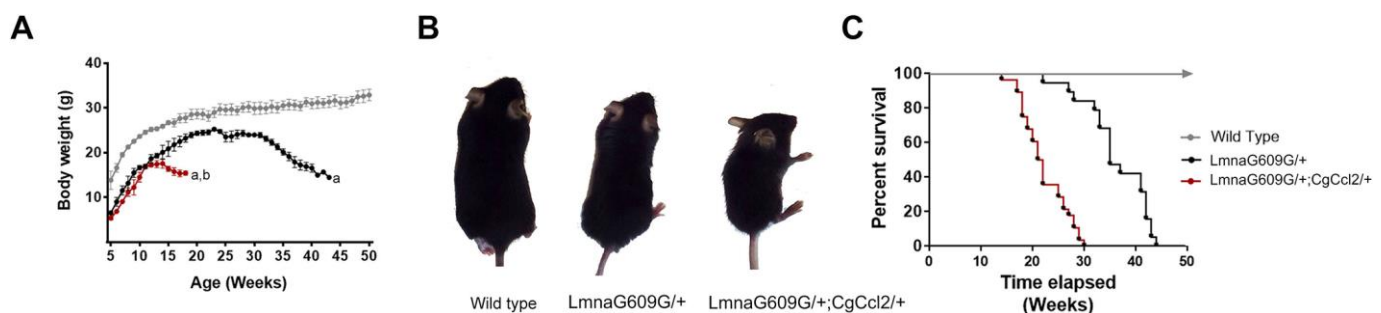
Figure 1. *Ccl2* significantly reduced the lifespan of mice with accelerated aging. *Ccl2* overexpression was critical for (**A**) the differential progression in body weight with age, (**B**) development of features of accelerated aging, as shown in the representative photographs of mice at 20 weeks of age, and (**C**) reduced lifespan, as shown by Kaplan-Meier survival plots from the wild-type (n=20), LMNAG609G/+ (*n=28)* and LMNAG609G/+;CGCCL2+/- (n=34) mice. LMNAG609G/+;CGCCL2+/- and LMNAG609G/+ denote progeroid mice overexpressing and not overexpressing Ccl2, respectively.

Degenerative cardiovascular changes, cachexia and sarcopenia also developed earlier in the LMNAG609G/+;CGCCL2+/- mice than in LMNAG609G/+ mice. The progeroid strains showed major histological alterations in the aorta and femoral arteries with respect to the controls. The extent of arterial fibrosis was greater in the LMNAG609G/+;CGCCL2+/- and LMNAG609G/+ mice than in the controls. Although the expression of actin and the number of stained macrophages were significantly higher in the mice with overexpressing *Ccl2*, the differences in fibrosis between the progeroid strains did not reach statistical significance (Supplementary Figure 1). The histological structure of the cardiac muscles in the progeroid mice was also significantly altered, and the changes were immediately apparent with routine staining procedures. Increased fibrosis of cardiac muscles was the most prominent feature caused by *Ccl2* overexpression (Supplementary Figure 2). Similarly, the generalized loss of fat depots and the extent of the abnormal structure of brown and epididymal white adipose tissue were significantly greater in the mice overexpressing *Ccl2*. In the tissues from both progeroid mouse strains, the adipocyte area was lower with higher expression of uncoupling protein one and an increased number of stained F4/80 cells compared to these levels in the controls. All these features and fibrosis were significantly affected by *Ccl2* overexpression (Supplementary Figure 3). The sarcopenia and cachexia causing the skeletal muscle loss in the genetically modified mice were significantly altered by *Ccl2* overexpression. The histological changes in both models of accelerated aging showed that fibrosis was significantly enhanced, but the response against oxidation was decreased, and the number of anti-inflammatory macrophages in muscle was significantly lower compared to those of the controls (Figure 2). The data indicate that *Ccl2* overexpression promoted death in mice with accelerated aging and confirmed the role of *Ccl2* as a fibrosis-inducing agent with a negative impact on biological outcomes associated with aging and/or longevity. A caveat of this set of experiments suggests that the ages at which the animals were studied differed for each experimental group (38-40 weeks for WT, 32 weeks for LMNAG609G/+, 18-22 weeks for LMNAG609G/+;CGCCL2+/-), since we decided to sacrifice the animals when they presented a similar degree of senescence, according to the criteria described in Materials and Methods. The age difference could explain, at least partially, the difference in the results that we observed in the arteries.

***Ccl2* overexpression drove specific signatures of metabolic dysregulation in the skeletal muscles of the progeroid mice**

To better understand the changes induced by lamin A mutation, we first performed a metabolomic analysis in muscle from fasted LMNAG609G/+ and WT mice. We selected this tissue due to its important implications in aging development. Metabolites from energy balancing and 1-C metabolism were quantitatively assessed, and normalized concentrations from all strains are depicted in Supplementary Tables 1, 2. The sets of metabolites studied demonstrated a clear distinction between LMNAG609G/+ and the controls. The partial least square discriminant analysis and the heatmap showed a clear distinction between animals from both groups (Supplementary Figure 4). The examination of individual metabolites showed that the LMNAG609G/+ animals had increased concentrations of compounds involved in energy metabolism. Notably, the increase in the concentrations of metabolites related to glycolysis, the analyzed amino acids, and the anaplerotic reactions in the CAC was important. 1-C metabolism was also altered in these mice, and the methionine level was significantly increased with a decrease in 5-methyl-tetrahydrofolate (5-methyl-THF), S-adenosylmethionine (SAM) and S-adenosylhomocysteine (SAH) levels, although we did not observe any significant alterations in DNA methylation (Figure 3B). These data likely indicate a combined defective function in the folate and methionine cycles.

The relative impact on the concentrations of these metabolites was different in the LMNAG609G/+;CGCCL2+/- mice than it was in the controls (Supplementary Figure 5). The main alterations observed were an increase in branched-chain amino acids (valine, isoleucine and leucine), β-hydroxybutyrate, fructose 1,6-bisphosphate, glucose 6-phosphate and ribose-5-phosphate concentrations, together with a depletion in 3-phosphoglycerate and citrate-isocitrate. Regarding 1-C metabolism, we observed an increase in riboflavin and methionine levels and a decrease in 5-methyl-THF, S-adenosylmethionine (SAM) and SAH. These alterations in 1-C metabolism induced an increase in the percentage of 5-methylcytosine (5-mC), which is a marker of DNA methylation. Interestingly, with respect to the controls, in both progeroid strains, the accumulation of the amino acids valine, leucine and isoleucine was significant.

We finally compared the metabolic alterations of LMNAG609G/+-;CGCCL2+/- with those of LMNAG609G/+, and we found a significant impact on the amount of metabolites in skeletal muscle that distinguished the strains, according to the results of the principal component analysis (Figure 3). Regarding energy metabolism, the LMNAG609G/+;CGCCL2+/- mice showed alterations in the glucose and citric acid cycles without significant alterations in amino acid concentrations with respect to the LMNAG609G/+ mice. In relation to 1-C metabolism, the LMNAG609G/+;CGCCL2+/- mice showed the downregulation of methionine, choline-dimethylglycine, 5 methyl-THF and

5 formyl-THF. These alterations may have been a consequence of the increase in SAM, SAH and AMP levels that we found in these animals. One of the most important consequences of SAM to SAH alterations was the increase in 5-mC. These findings might be relevant because they strongly suggest alterations in muscle DNA methylation and demethylation. DNA methyltransferases use SAM as a substrate to produce SAH; DNA demethylation depends on α-ketoglutarate and other metabolites from the CAC [24]. *Ccl2* overexpression
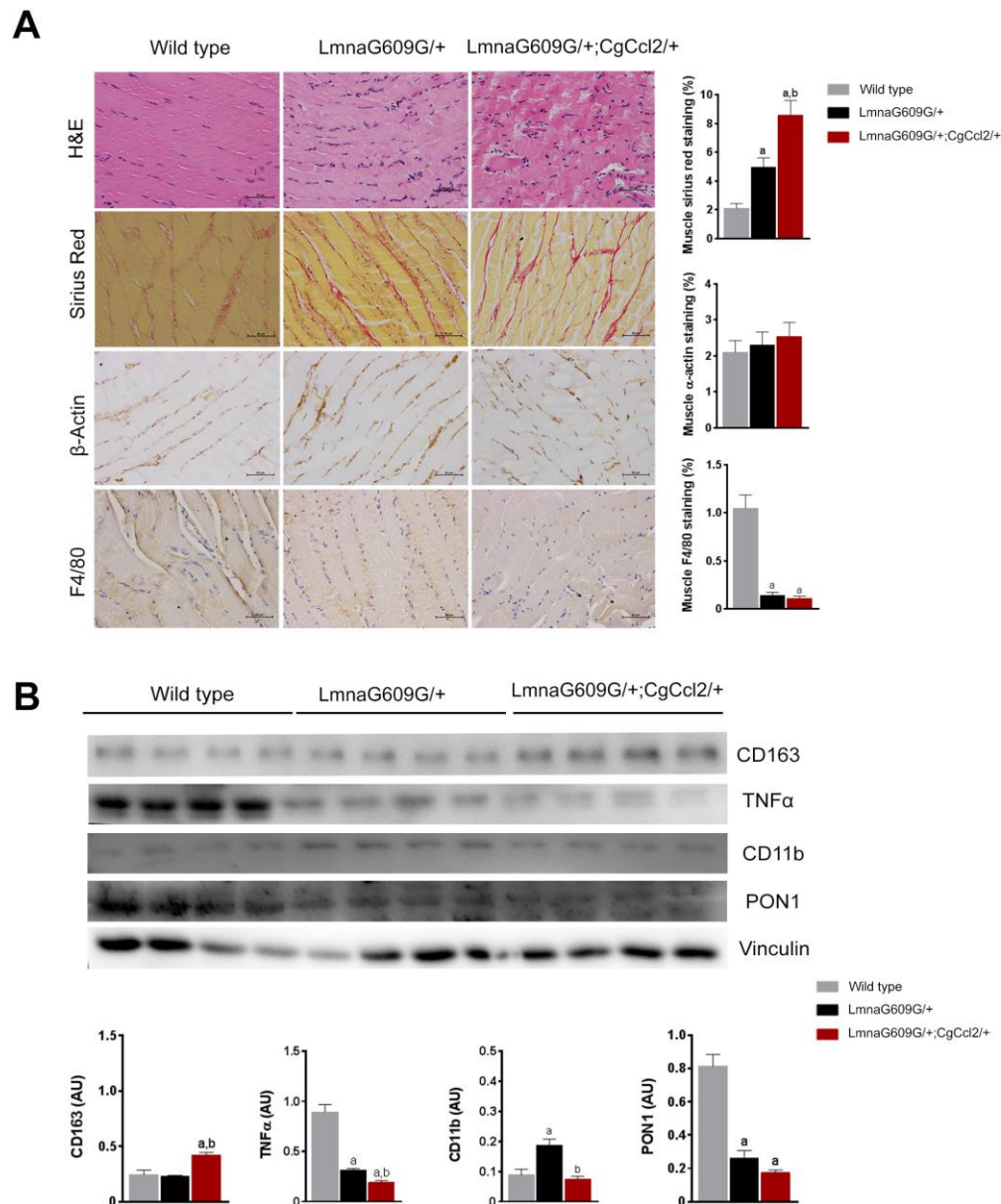
Figure 2. Histological phenotypes were altered in the muscles of aged mice. The structural changes in quadriceps muscles are depicted in representative micrographs of tissue stained with hematoxylin and eosin and Sirius red staining and determined by immunohistochemical analysis of β-actin and F4/80 cells. *Ccl2* overexpression accelerated the presence of histological alterations (**A**). Fibrosis was a prominent feature in the progeroid mice, but the relative amount of actin-stained cells was similar among strains, despite major differences in muscle weight. Interestingly, the number of F4/80-stained cells was significantly lower in the progeroid mice. We then used immunoblotting to examine (**B**) the expression of the markers of macrophage polarization, including cluster of differentiation (CD) 11 and 163, and tumor necrosis factor (TNFα) to indicate the relative anti-inflammatory activity, which was accompanied by lower expression of the major antioxidant enzyme paraoxonase 1 (PON1) in both progeroid strains. The LMNAG609G/+;CGCCL2+/- mice were compared with wild-type mice, as depicted by [a] p<0.05, and with LA [+/-] mice, as depicted by [b] p<0.05, according to the Mann–Whitney U tests (n=15 for each strain). LMNAG609G/+;CGCCL2+/- and LMNAG609G/+ denote progeroid mice overexpressing and not overexpressing Ccl2, respectively.

significantly increased the methylation of cytosine bases in muscle DNA and significantly decreased 5-hmC levels with respect to both the LMNAG609G/+ mice and controls (Figure 3C). Taken together, our data indicate that *Ccl2* overexpression in the experimental model of progeria alters energy and 1-C metabolism and drives dynamic changes in DNA methylation. The role of these epigenetic marks remains to be ascertained.

Ccl2 overexpression disrupted mitochondrial dynamics and altered AMPK/m-TOR-driven pathways in the progeroid mice

Our data might suggest key roles of mitochondrial metabolites in pathological aging. Although the mechanisms are uncertain, *Ccl2* overexpression interferes with mitochondrial function, particularly in the oxidative phosphorylation system (OXPHOS) and the production of ATP and reactive oxygen species (ROS) [25]. Indeed, our group previously reported that transgenic mice with a WT background that overexpress Ccl2 show alterations in mitochondrial morphology; therefore, the matrix is less electron-dense. We also found altered fusion dynamics. In transgenic mice fed a chow diet, a tendency of the unbalanced dynamics shifted towards mitochondrial fusion, but dietary manipulation elicited a significant shift towards fission. These putative mechanisms of the altered metabolism seem to be related to the autophagic response [20].

We therefore explored the expression of the mitochondrial respiratory complexes in skeletal muscle. Complexes I and II are major players in mitochondrial signaling and ROS generation, and their expression was significantly decreased in the progeroid mice compared with that of the controls. The expression levels, especially of complex I, were lower in the LMNAG609G/+;CGCCL2+/- mice than in the LMNAG609G/+ mice. Additionally, complexes III and IV appeared normal in the muscles of the LMNAG609G/+ mice with respect to the muscles of the controls, but *Ccl2* overexpression in the LMNAG609G/+;CGCCL2+/- mice significantly decreased complex expression. Finally, the expression of complex V (ATP synthase) in the muscles of the LMNAG609G/+ mice was significantly decreased, and this effect was significantly more prominent in the LMNAG609G/+;CGCCL2+/- mice. In addition, the protein concentrations of translocase of outer membrane 20 (TOM20) and mitofusin 2 (MFN2) in the muscles of the progeroid mice were decreased, indicating alterations in the proper formation of the mitochondrial network (Figure 4A).

Ccl2 overexpression had a negative impact on the cellular bioenergetics in progeroid skeletal muscle, and this negative effect was associated with reduced efficiency of mTOR-related homeostatic mechanisms. In the muscles of the LMNAG609G/+ mice, the expression and phosphorylation of p53 was increased with respect to that of the controls, and the level of p53 activation in the LMNAG609G/+;CGCCL2+/- mice was significantly increased with respect to that in the LMNAG609G/+ mice, which likely indicates the triggering of aging through a p53-mediated transcriptional program. As p53 is a major factor in the cell cycle and proliferation and because senescent cells may be more or less metabolically active, the differential response may be the result of the differences in the expression and activation of related molecules, most likely those associated with the mechanistic target of rapamycin (mTOR). We explored major upstream and downstream pathway players and found that the phosphoinositide 3-kinase (PI3K)/AKT (also known as protein kinase B) pathway, with critical roles in regulating diverse cellular functions, was abnormal. PI3K and AKT expression was not affected in the cells of either the progeroid or the *Ccl2*-overexpressing strains. However, AKT was not phosphorylated at S473 in the muscle cells of either progeroid mouse strain, and S6 phosphorylation was significantly decreased in the LMNAG609G/+ mice and undetectable in the LMNAG609G/+;CGCCL2+/- mice, indicating that mTOR signaling is significantly inhibited in these models of accelerated aging. AMP-activated protein kinase (AMPK) expression was significantly lower in the cells of the genetically modified mice, but its relative phosphorylation was significantly higher. The effect was more pronounced in the LMNAG609G/+;CGCCL2+/- mice than in LMNAG609G/+ mice. The cells overexpressing *Ccl2* in the LMNAG609G/+;CGCCL2+/- mice apparently favored autophagy with respect to the cells in the LMNAG609G/+ mice, as indicated by a higher LC3II/I ratio. However, the expression levels of the lysosomal membrane proteins LAMP2A and p62 were decreased in the progeroid mice, suggesting the involvement of chaperone-mediated autophagy in aging and the ability of *Ccl2* to interfere in this process (Figure 4B). However, we cannot verify that CCL2 decreases ATP levels AMPK or, in contrast, AMPK is activated because of other changes, such as the upregulation of Ca^{2+} levels.

DISCUSSION

The activation of the immune machinery critical for chronic inflammation has been associated with age-related diseases and the process of aging [2, 3, 26]. There is no clear understanding of the mechanisms that initiate this relationship, but several common molecular pathways have been identified through their characteristic increase in senescent cells during aging [27]. Senescent cells secrete factors that include chemokines, which have complex effects on the trafficking of immune cells
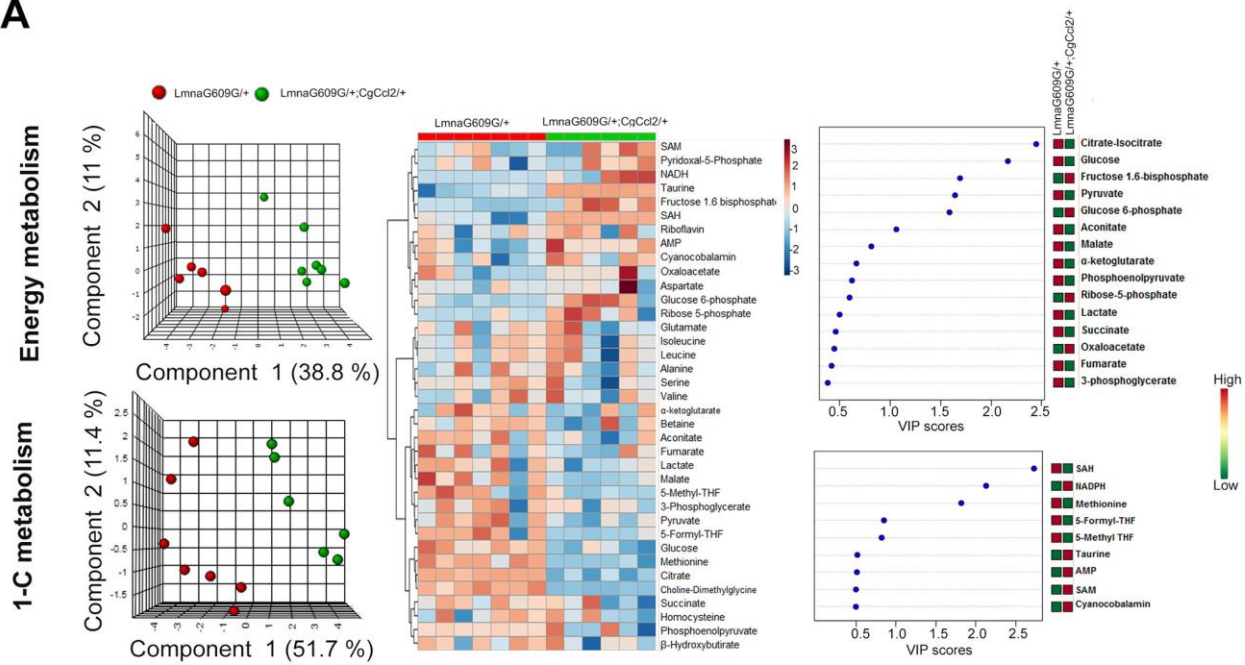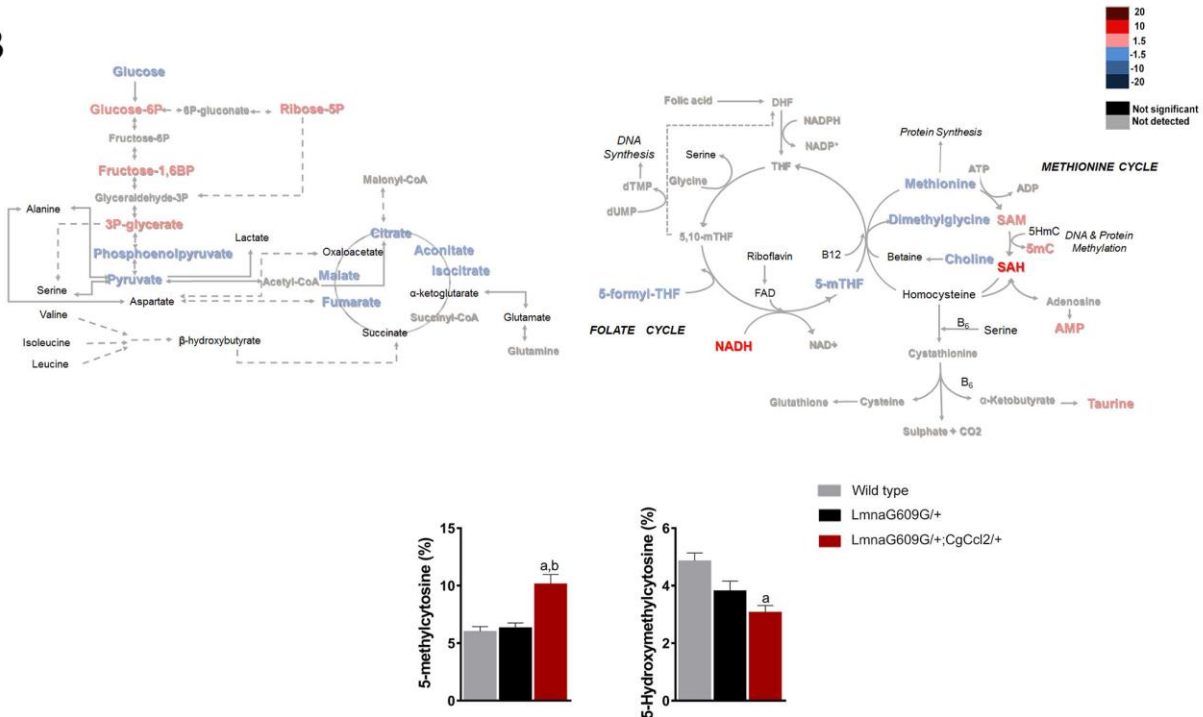
Figure 3. The impact of *Ccl2* overexpression on the metabolic pathways associated with energy and 1-C metabolism. Metabolomic analysis of skeletal muscle from progeroid mice with (LMNAG609G/+;CGCCL2+/-) or without (LMNAG609G/+) increased *Ccl2* levels revealed the metabolic impact of *Ccl2* in accelerated aging. (**A**) From left to right, partial least square discriminant analysis (PLSDA), heatmap with hierarchical clustering and random forest analysis indicating that *Ccl2* drove changes in energy and 1-C metabolism in the quadriceps muscles of the genetically modified mice. The levels of metabolites were distinct in both strains, and the variables of highest importance, according to the projection scores, were glucose, citrate, SAH and methionine. (**B**) Comparison of the levels of metabolite abundance from glycolysis and the CAC cycle in the quadriceps muscles were assessed by fold changes, as indicated in the legend, suggesting that Ccl2 decreased mitochondrial oxidative metabolism. (C) Dysregulation in the methionine cycle was, at least partially, the cause of the increased DNA methylcytosine levels in the LMNAG609G/+;CGCCL2+/- mice with respect to the controls and LMNAG609G/+ mice. Values are shown as the means ± SEM; [a]p< 0.05 with respect to the wild-type mice and [b] p<0.05 with respect to the LMNAG609G/+ mice, according to the Mann–Whitney U tests.
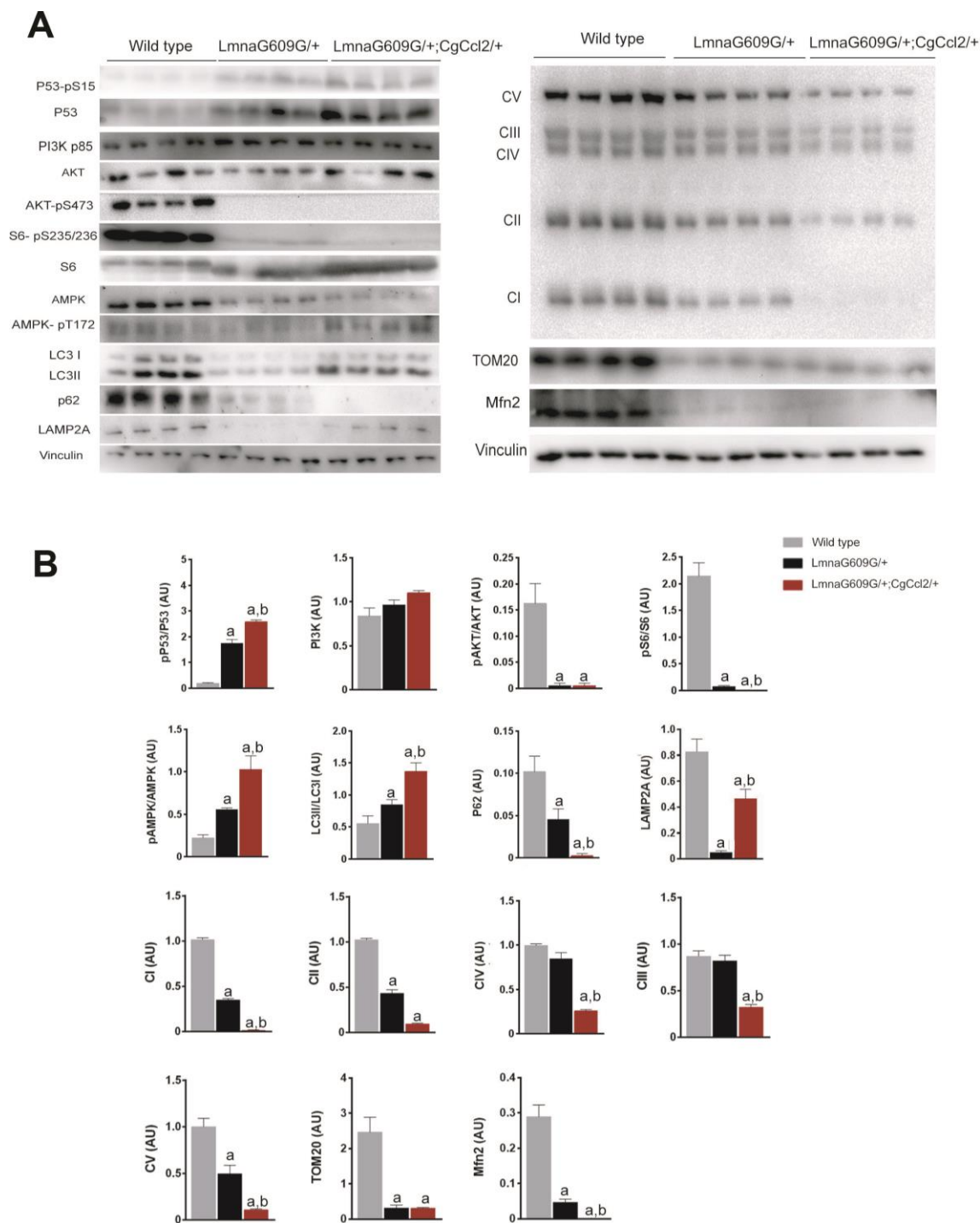
Figure 4. Ccl2 overexpression significantly altered the expression of the complexes related to oxidative phosphorylation and the relevant metabolic signaling pathways in the quadriceps muscle. Ccl2 overexpression exacerbated the metabolic reduction, mainly in mitochondria, (**A**) of the mice with accelerated aging and altered (**B**) the functioning of AMPK-mTOR-driven pathways. LMNAG609G/+;CGCCL2+/- and LMNAG609G/+ denote progeroid mice overexpressing and not overexpressing Ccl2, respectively. Values are shown as the means ± SEM; [a] p< 0.05 with respect to the wild-type mice and [b] p<0.05 with respect to the LMNAG609G/+ mice according to the Mann–Whitney U tests. Acronyms in (**A**) denote complex I or NADH/ubiquinone oxidoreductase, complex II or succinate dehydrogenase, complex III or cytochrome C reductase, complex IV or cytochrome C oxidase, complex V or ATP synthase, translocase of outer membrane (TOM20), and mitofusin 2 (Mfn2); acronyms in (**B**) phospho-tumor suppressor p53 (p53-pS15), tumor suppressor p53 (P53), phosphoinositide 3-kinase (PI3K), protein kinase B (AKT) and phospho-protein kinase B (AKT-pS473), phospho-ribosomal protein S6 (S6-pS235/236), ribosomal protein S6 (S6), AMPK activated protein kinase (AMPK), phospho-AMPK activated protein kinase (AMPK pT172), microtubule-associated proteins 1A/1B light chain 3B (LC3), p62 adaptor protein or sequestosome 1, and lysosome-associated membrane protein 2 (LAMP2A).

[13, 28]. Epidemiological studies have suggested that chemokine levels are increased in aged individuals, particularly Ccl2, with or without metabolic alterations, and *in vitro*, they appear to confer senescence even to neighboring normal cells in an autocrine and paracrine fashion [18, 29, 30]. The ubiquitous expression of *Ccl2* in aged tissues suggests a potentially important role, but the analysis and interpretation remain complicated by the joint expression of functional and atypical receptors and antioxidant enzymes [31]. We previously studied the effect of only *Ccl2* overexpression in mice with a WT background [20]. The mice resulting from the targeted mutation were viable, fertile and normal in size and weight and showed no apparent behavioral or reproductive defects. We also found that the mutant mice died prematurely between 10 and 14 months when given a high-fat diet but not when given a normal diet. Furthermore, we also reported that *Ccl2*-deficient mice were protected from oxidative stress, inflammation and metabolic disturbances and had a normal lifespan [15]. To investigate the prosenescence effects of *Ccl2* in accelerated aging at the organismal level, we developed an experimental model that combines progeria induced by a mutation in the *Lmna* gene and systemic *Ccl2* overexpression. The results indicated that excessive *Ccl2* promoted the death of the mice with progeria. *Ccl2* overexpression reduced the average mouse lifespan, accelerated the development of premature degenerative changes and caused metabolic dysregulation. The mechanisms are likely multifaceted but appear to be independent, at least partially, from their roles as chemoattractants because macrophages did not significantly accumulate in all the tissues. The cause of death was unclear, but *Ccl2* overexpression was a significant promoter of fibrosis in all the tissues.

Dysregulation of certain metabolites may lead to altered cell function, including immune cells, in a model characterized by increased accumulation of progerin [23]. Progerin is a mutant protein in the nuclear lamina encoded by the *Lmna* gene and has been linked to multiple clinical pathologies, including the skeletal myopathies and premature aging observed in HPGS [32]. In mice, the conditional overexpression of progerin in muscle induced multiple metabolic defects and premature death, indicating an intrinsic effect of progerin on energy metabolism and aging [33, 34]. Muscle metabolites from energy and 1-C metabolism revealed major alterations in energy expenditure and mitochondrial dynamics in the $Lmna^{+/-}$ mice, and these outcomes were negatively affected by *Ccl2* overexpression. Specifically, *Ccl2* contributed to the mitochondrial dysfunction and impairment of cellular bioenergetics in the muscles of the progeroid mice with complex metabolic alterations, which may have affected cellular survival,

autophagy and protein synthesis, possibly contributing to the histological alterations and decreased mouse lifespan. The molecular damage caused by increases in progerin [35] emerged when the cumulative damage caused by accelerated aging was not ameliorated by compensating homeostatic mechanisms. The impact of *Ccl2* overexpression likely included the impairment of these compensatory mechanisms and, in particular, a reduction in the adaptation of mitochondrial function in the mice with accelerated aging. It was noticeable that progeria and *Ccl2* overexpression increased methionine levels in the muscles and altered the DNA methylation status, likely with associated epigenetic changes. Our experimental model combined the impairment of mitochondrial function and dysregulation in methionine metabolism that altered SAM and SAH levels [36]. Interestingly, high methionine levels in human diseases are associated with profound alterations in muscle [37], and dietary methionine restriction, which in progeroid mice decreased inflammation and enhanced mitochondrial activity, has been associated with increased lifespan [38].

One of the most characterized senescence markers is p53, which we found to be increased in both progeroid mouse strains. The interactions between p53 and mTORC1 are regulated by several factors. For instance, it has been demonstrated that p53 induces the direct or indirect activation of AMPK, which is considered to be one of the most important inhibitors of mTORC1. Moreover, p53 also induces the PTEN/PI3K/AKT pathway to reduce mTORC1 activity [39]. This metabolic reprogramming causes systemic alterations in cells, such as upregulated autophagy. Autophagy promotes the recycling of damaged organelles in response to metabolic alterations or nutrient depletion [40–42] and is considered to be one of the most important anti-aging mechanisms of cells. Interestingly, we observed an increase in macroautophagy in both groups of progeroid mice despite their accelerated aging. Similar results were observed using mouse models of progeria [43, 44]. We suggest that macroautophagy activation is an adaptive response to the metabolic stress observed in these mice. Moreover, upregulated macroautophagy may be a compensatory mechanism to attenuate the chaperone-mediated autophagy impairment (CMA) observed in both groups. The downregulation of CMA is associated with loss of protein degradation machinery [45], a finding that may explain the increase in amino acid concentrations observed in the LMNAG609G/+;CGCCL2+/- and LMNAG609G/+ mice. A decline in protein homeostasis is closely related to aging progression and degenerative diseases such as Alzheimer's disease, Parkinson's disease, Huntington's disease and cancer [45].

Mitochondrial function, autophagy, and glycolysis are closely linked and related to each other in a complex manner that is not yet well understood. Our results show activation of glycolysis in mice that overexpress Ccl2 despite the inactivation of the mTORC1 system. We do not know the alternative mechanism that explains this phenomenon, but it is known that p53 regulates many aspects of metabolism, such as glycolysis, mitochondrial oxidative phosphorylation and gluta-minolysis, and we think that this pathway should be explored in subsequent studies.

In conclusion, our findings indicate that *Ccl2* signaling promotes death and negatively impacts the energetic balance and muscle homeostasis in mice with lamin A mutations and accelerated aging. In this study, we describe an animal model that combines the overexpression of *Ccl2* in mice with a progeroid background, and we report that these animals present important metabolic alterations in muscle tissue. Our data are preliminary and support previously obtained results [18, 46], suggesting that the secretion of *Ccl2* by senescent cells correlates with biological age and may be used as a therapeutic target or as a biomarker aimed at monitoring the efficacy of interventions that extend healthy aging. Further studies are necessary to elucidate the mechanisms underlying these alterations.

MATERIALS AND METHODS

Animals and experimental design

Genetically modified mice that overexpress *Ccl2* (*CgCcl2*) were generated in our laboratory as described [20]. The mice with the *Lmna ^{G609G}* mutation (LA), which constitutes a model of accelerated aging and progeria, were generated at the University of Oviedo [23]. Crossbreeding resulted in the first progeny (F1) of heterozygous animals with the LMNAG609G/+ mutation and *Ccl2* overexpression in tissues (LMNAG609G/+;CGCCL2+/-), which was confirmed by routine genotyping and *Ccl2* measurements (n = 34). In the LMNAG609G/+ mice, the *Ccl2* concentrations in tissues were similar to those observed in the controls, except in adipose tissues, but the *Ccl2* levels in the LMNAG609G/+;CGCCL2+/- mice were significantly higher in all tissues. The second progeny (F2) of the LMNAG609G/+;CGCCL2+/- mice were not fertile, and consequently, homozygotes for the two characteristics were not available. Wild-type (WT) (n = 20) and LMNAG609G/+ mice (n = 28) were used as controls (Supplementary Figure 6). The mice were fed a normal standard diet from Scientific Animal Food & Engineering (SAFE, Augy, France) and water ad libitum for the duration of the experiments and maintained under controlled temperature (22° C), humidity (50%) and a light/dark cycle (12 h/12 h). The animal procedures were approved by the Ethics Review Committee for Animal Experimentation of (protocols 10281 and FUE-2018-00849209) and designed according to European guidelines (Directive 2010/63/EU).

The mice included in the study were male with a C57BL/6J genetic background, used at 4 weeks of age and assessed daily for lifespan indicators with manipulation maintained at a minimum. To avoid unnecessary suffering and to ensure the lack of bias, we established strict criteria for the decision to sacrifice that was based on a previously reported grading score of senescence (Supplementary Table 3) [47].

Tissue collection, the preparation of extracts and Ccl2 measurements

All tissues were collected upon mouse sacrifice, and selected pieces were frozen and stored at -80° C until batch analyses. Portions of each 30 mg sample of liver, pancreas, skeletal muscle (from quadriceps muscles), heart, major arteries (aorta and femoral) and brown and epididymal white adipose tissue were homogenized using a sonicator (Branson Sonifer 150, Thistle Scientific, Glasgow, UK) in 50 mM Tris, 1 mM EDTA, 1% IGEPAL CA-630, 150 mM NaCl, 0.10% Triton, 50 mM NaF, 100 mM phenylmethanesulfonyl fluoride (PMS) and 1 mM Na_3VO_4. Protein concentration was determined with the Pierce BCA protein assay kit. To measure *Ccl2* by ELISA (PeproTech, London, UK), following the manufacturer's instructions, 200 µg of protein from each extract was used.

Histological analysis and immunohistochemistry

Separate portions of the same tissues were collected in formalin (3.7-4% formaldehyde buffered to pH 7 and stabilized with 1-1.5% methanol) and embedded in paraffin. Hematoxylin and eosin and Sirius red staining were used for each tissue. At least 10 sections per mouse were assessed, and the tissue was blindly evaluated to assess defects in structure and detect fibrosis. For immunohistochemistry, antigens were retrieved in Tris 10 mM/EDTA 1 mM buffer at pH 9 in a microwave oven that reached 90° C. Bovine serum albumin (2%) and hydrogen peroxide (1%) were sequentially used to block nonspecific binding sites and endogenous peroxidase, and the sections were rinsed with phosphate-buffered saline. Then, the sections were incubated with primary and secondary antibodies (Supplementary Table 4). All sections were counterstained with Mayer's hematoxylin and quantified (at least 10 fields for each sample) using ImageJ software.

Immunoblot analysis

Frozen tissues from each mouse were homogenized in lysis buffer containing 50 mM Tris at pH 7.4, 1 mM EDTA, 1% IGEPAL CA-630, 150 mM NaCl, 0.10% Triton, 50 mM NaF, 100 mM phenylmethanesulfonyl fluoride and 1 mM Na_3VO_4. Protein concentration was determined, and the samples were denatured in Laemmli buffer with β-mercaptoethanol at 100° C for 5 min, and 50 µg was loaded per lane onto 8%-14% sodium dodecyl sulfate-polyacrylamide gels. The gels were then transferred to polyvinylidene difluoride or nitrocellulose membranes, blocked with 5% nonfat dry milk or bovine serum albumin in 20 mM Tris at pH 7.4, 150 mM NaCl and 1% Tween-20, and incubated with the respective antibodies (Supplementary Table 4). Immunoreactive bands were developed with a SuperSignal West Femto chemiluminescent substrate (Pierce, Rockford, IL, USA) in a ChemiDoc system (Bio-Rad Laboratories, Madrid, Spain). The bands were quantified using Image Lab 2.0 software (Bio-Rad Laboratories, Hercules, CA, USA).

Quantitative metabolomics platform and chromatographic procedures

Targeted metabolomics analysis was performed as reported with some modifications [48]. To limit variability, batch analysis was required, and the number of samples measured per day was restricted to n = 24 (n = 8 for each strain). To measure the metabolites of energy metabolism, the tissues were homogenized using a Precellys 24 homogenizer (Izasa, Barcelona, Spain) in 1 mL of methanol/water (8:2) and D4-succinic acid and stored at -20° C for 2 h to precipitate the proteins. After centrifugation at 15,000 rpm for 10 min at 4° C, the supernatants were dried under N_2 and derivatized with methoxyamine hydrochloride dissolved in pyridine (40 mg/mL) and N-methyl-N-trimethylsilyl trifluoroacetamide. We used a 7890A gas chromatograph coupled with an electron impact source to a 7200 quadrupole time-of-flight mass spectrometer (Agilent Technologies, Santa Clara, USA). For measuring metabolites of 1-C metabolism, tissues were added to 1 mL of an extraction solution containing methanol:water (8:2 v/v), 1% ascorbic acid (m/v) and 0.5% β-mercaptoethanol (v/v) and homogenized with a Precellys 24 homogenizer (Izasa). After protein precipitation, the samples were centrifuged, and the supernatants were dried under N_2 and then resuspended in ultrapure water containing 50 mM ammonium acetate and 0.2% formic acid. The analysis was performed with an ultra-high pressure liquid chromatography-quadrupole time-of-flight mass spectrometer (Agilent Technologies). Liquid chromatography was also used in separate analyses to quantitate guanine, 5-methylcytosine (5-mC) and 5-hydroxymethylcytosine (5-hmC) as described [49].

Statistical analyses

The statistical comparisons were performed using nonparametric Mann-Whitney U tests with IBM SPSS Statistics for Windows, Version 21 (Armonk, NY, USA, IBM Corp.). Metabolites were quantitated in all the samples using MassHunter Quantitative Analysis B.07.00 software (Agilent Technologies) according to the calibration curve of the corresponding standard. Partial least squares-discriminant analysis (PLS-DA), hierarchical clustering and the variable importance in the projection score were calculated with MetaboAnalyst 4.0 (https://www.metaboanalyst.ca) software [50]. GraphPad Prism 6.01 software (GraphPad Software, San Diego, CA) was also used for relevant statistical confirmation and graphics. Differences were considered statistically significant when the p value was ≤ 0.05. Unless otherwise indicated, the results are expressed as the means ± standard error of the mean.

AUTHOR CONTRIBUTIONS

Fedra Luciano-Mateo, Javiar A. Menéndez, Jordi Camps, and Jorge Joven contributed to conception and design of the experimental plan. Fedra Luciano-Mateo, Noemí Cabré, Gerard Baiges-Gaya, Salvador Fernández-Arroyo, Anna Hernández-Aguilera, Elisabet Rodríguez-Tomàs, Meritxell Arenas, and Javier A. Menéndez made substantial contributions to acquisition, analysis and interpretation of data. Fedra Luciano-Mateo, Jordi Camps and Jorge Joven wrote the draft and all authors contributed to the final manuscript.

CONFLICTS OF INTEREST

There are no conflicts of interest associated with this report.

REFERENCES

1. Franceschi C, Garagnani P, Parini P, Giuliani C, Santoro A. Inflammaging: a new immune-metabolic viewpoint for age-related diseases. Nat Rev Endocrinol. 2018; 14:576–90.
https://doi.org/10.1038/s41574-018-0059-4
PMID:30046148

2. López-Otín C, Blasco MA, Partridge L, Serrano M, Kroemer G. The hallmarks of aging. Cell. 2013; 153:1194–217.
https://doi.org/10.1016/j.cell.2013.05.039
PMID:23746838

3. Fulop T, Witkowski JM, Olivieri F, Larbi A. The integration of inflammaging in age-related diseases. Semin Immunol. 2018; 40:17–35.
https://doi.org/10.1016/j.smim.2018.09.003
PMID:30287177

4. Miller RA, Harrison DE, Astle CM, Floyd RA, Flurkey K, Hensley KL, Javors MA, Leeuwenburgh C, Nelson JF, Ongini E, Nadon NL, Warner HR, Strong R. An aging interventions testing program: study design and interim report. Aging Cell. 2007; 6:565–75.
https://doi.org/10.1111/j.1474-9726.2007.00311.x
PMID:17578509

5. Baker GT 3r, Sprott RL. Biomarkers of aging. Exp Gerontol. 1988; 23:223–39.
https://doi.org/10.1016/0531-5565(88)90025-3
PMID:3058488

6. Jylhävä J, Pedersen NL, Hägg S. Biological age predictors. EBioMedicine. 2017; 21:29–36.
https://doi.org/10.1016/j.ebiom.2017.03.046
PMID:28396265

7. Barzilai N, Crandall JP, Kritchevsky SB, Espeland MA. Metformin as a tool to target aging. Cell Metab. 2016; 23:1060–65.
https://doi.org/10.1016/j.cmet.2016.05.011
PMID:27304507

8. Menendez JA, Joven J. One-carbon metabolism: an aging-cancer crossroad for the gerosuppressant metformin. Aging (Albany NY). 2012; 4:894–98.
https://doi.org/10.18632/aging.100523 PMID:23525940

9. Menendez JA, Cufí S, Oliveras-Ferraros C, Vellon L, Joven J, Vazquez-Martin A. Gerosuppressant metformin: less is more. Aging (Albany NY). 2011; 3:348–62.

https://doi.org/10.18632/aging.100316
PMID:21483040

10. Horvath S. DNA methylation age of human tissues and cell types. Genome Biol. 2013; 14:R115.
https://doi.org/10.1186/gb-2013-14-10-r115
PMID:24138928

11. Horvath S, Raj K. DNA methylation-based biomarkers and the epigenetic clock theory of ageing. Nat Rev Genet. 2018; 19:371–84.
https://doi.org/10.1038/s41576-018-0004-3
PMID:29643443

12. Irvin MR, Aslibekyan S, Do A, Zhi D, Hidalgo B, Claas SA, Srinivasasainagendra V, Horvath S, Tiwari HK, Absher DM, Arnett DK. Metabolic and inflammatory biomarkers are associated with epigenetic aging acceleration estimates in the GOLDN study. Clin Epigenetics. 2018; 10:56.
https://doi.org/10.1186/s13148-018-0481-4
PMID:29713391

13. Berent-Maoz B, Montecino-Rodriguez E, Signer RA, Dorshkind K. Fibroblast growth factor-7 partially reverses murine thymocyte progenitor aging by repression of Ink4a. Blood. 2012; 119:5715–21.
https://doi.org/10.1182/blood-2011-12-400002
PMID:22555975

14. Menendez JA, Cufí S, Oliveras-Ferraros C, Martin-Castillo B, Joven J, Vellon L, Vazquez-Martin A. Metformin and the ATM DNA damage response (DDR): accelerating the onset of stress-induced senescence to boost protection against cancer. Aging (Albany NY). 2011; 3:1063–77.
https://doi.org/10.18632/aging.100407
PMID:22170748

15. Luciano-Mateo F, Cabré N, Fernández-Arroyo S, Baiges-Gaya G, Hernández-Aguilera A, Rodríguez-Tomàs E, Mercado-Gómez M, Menendez JA, Camps J, Joven J. Chemokine (C-C motif) ligand 2 gene ablation protects low-density lipoprotein and paraoxonase-1 double deficient mice from liver injury, oxidative stress and inflammation. Biochim Biophys Acta Mol Basis Dis. 2019; 1865:1555–66.
https://doi.org/10.1016/j.bbadis.2019.03.006
PMID:30905786

16. Palmer AK, Xu M, Zhu Y, Pirtskhalava T, Weivoda MM, Hachfeld CM, Prata LG, van Dijk TH, Verkade E, Casaclang-Verzosa G, Johnson KO, Cubro H, Doornebal EJ, et al. Targeting senescent cells alleviates obesity-induced metabolic dysfunction. Aging Cell. 2019; 18:e12950.
https://doi.org/10.1111/acel.12950 PMID:30907060

17. Coppé JP, Desprez PY, Krtolica A, Campisi J. The senescence-associated secretory phenotype: the dark

side of tumor suppression. Annu Rev Pathol. 2010; 5:99–118.
https://doi.org/10.1146/annurev-pathol-121808-102144 PMID:20078217

18. Yousefzadeh MJ, Schafer MJ, Noren Hooten N, Atkinson EJ, Evans MK, Baker DJ, Quarles EK, Robbins PD, Ladiges WC, LeBrasseur NK, Niedernhofer LJ. Circulating levels of monocyte chemoattractant protein-1 as a potential measure of biological age in mice and frailty in humans. Aging Cell. 2018; 17:e12706.
https://doi.org/10.1111/acel.12706 PMID:29290100

19. Justice JN, Niedernhofer L, Robbins PD, Aroda VR, Espeland MA, Kritchevsky SB, Kuchel GA, Barzilai N. Development of clinical trials to extend healthy lifespan. Cardiovasc Endocrinol Metab. 2018; 7:80–83.
https://doi.org/10.1097/XCE.0000000000000159 PMID:30906924

20. Rodríguez-Gallego E, Riera-Borrull M, Hernández-Aguilera A, Mariné-Casadó R, Rull A, Beltrán-Debón R, Luciano-Mateo F, Menendez JA, Vazquez-Martin A, Sirvent JJ, Martín-Paredero V, Corbí AL, Sierra-Filardi E, et al. Ubiquitous transgenic overexpression of C-C chemokine ligand 2: a model to assess the combined effect of high energy intake and continuous low-grade inflammation. Mediators Inflamm. 2013; 2013:953841.
https://doi.org/10.1155/2013/953841 PMID:24453432

21. Carrero D, Soria-Valles C, López-Otín C. Hallmarks of progeroid syndromes: lessons from mice and reprogrammed cells. Dis Model Mech. 2016; 9:719–35.
https://doi.org/10.1242/dmm.024711 PMID:27482812

22. Merideth MA, Gordon LB, Clauss S, Sachdev V, Smith AC, Perry MB, Brewer CC, Zalewski C, Kim HJ, Solomon B, Brooks BP, Gerber LH, Turner ML, et al. Phenotype and course of Hutchinson-Gilford progeria syndrome. N Engl J Med. 2008; 358:592–604.
https://doi.org/10.1056/NEJMoa0706898 PMID:18256394

23. Osorio FG, Navarro CL, Cadiñanos J, López-Mejía IC, Quirós PM, Bartoli C, Rivera J, Tazi J, Guzmán G, Varela I, Depetris D, de Carlos F, Cobo J, et al. Splicing-directed therapy in a new mouse model of human accelerated aging. Sci Transl Med. 2011; 3:106ra107.
https://doi.org/10.1126/scitranslmed.3002847 PMID:22030750

24. Ren R, Ocampo A, Liu GH, Izpisua Belmonte JC. Regulation of stem cell aging by metabolism and epigenetics. Cell Metab. 2017; 26:460–74.
https://doi.org/10.1016/j.cmet.2017.07.019 PMID:28826795

25. Gordaliza-Alaguero I, Cantó C, Zorzano A. Metabolic implications of organelle-mitochondria communication. EMBO Rep. 2019; 20:e47928.
https://doi.org/10.15252/embr.201947928 PMID:31418169

26. Hotamisligil GS. Endoplasmic reticulum stress and the inflammatory basis of metabolic disease. Cell. 2010; 140:900–17.
https://doi.org/10.1016/j.cell.2010.02.034 PMID:20303879

27. Rea IM, Gibson DS, McGilligan V, McNerlan SE, Alexander HD, Ross OA. Age and age-related diseases: role of inflammation triggers and cytokines. Front Immunol. 2018; 9:586.
https://doi.org/10.3389/fimmu.2018.00586 PMID:29686666

28. Sierra-Filardi E, Nieto C, Domínguez-Soto A, Barroso R, Sánchez-Mateos P, Puig-Kroger A, López-Bravo M, Joven J, Ardavín C, Rodríguez-Fernández JL, Sánchez-Torres C, Mellado M, Corbí AL. CCL2 shapes macrophage polarization by GM-CSF and M-CSF: identification of CCL2/CCR2-dependent gene expression profile. J Immunol. 2014; 192:3858–67.
https://doi.org/10.4049/jimmunol.1302821 PMID:24639350

29. Acosta JC, Banito A, Wuestefeld T, Georgilis A, Janich P, Morton JP, Athineos D, Kang TW, Lasitschka F, Andrulis M, Pascual G, Morris KJ, Khan S, et al. A complex secretory program orchestrated by the inflammasome controls paracrine senescence. Nat Cell Biol. 2013; 15:978–90.
https://doi.org/10.1038/ncb2784 PMID:23770676

30. Lee JY, Yu KR, Lee BC, Kang I, Kim JJ, Jung EJ, Kim HS, Seo Y, Choi SW, Kang KS. GATA4-dependent regulation of the secretory phenotype via MCP-1 underlies lamin a-mediated human mesenchymal stem cell aging. Exp Mol Med. 2018; 50:1–12.
https://doi.org/10.1038/s12276-018-0092-3 PMID:29760459

31. Hernández-Aguilera A, Fibla M, Cabré N, Luciano-Mateo F, Camps J, Fernández-Arroyo S, Martín-Paredero V, Menendez JA, Sirvent JJ, Joven J. Chemokine (C-C motif) ligand 2 and coronary artery disease: tissue expression of functional and atypical receptors. Cytokine. 2020; 126:154923.
https://doi.org/10.1016/j.cyto.2019.154923 PMID:31739217

32. Janin A, Bauer D, Ratti F, Millat G, Méjat A. Nuclear envelopathies: a complex LINC between nuclear envelope and pathology. Orphanet J Rare Dis. 2017; 12:147.
https://doi.org/10.1186/s13023-017-0698-x PMID:28854936

33. Wang WP, Wang JY, Lin WH, Kao CH, Hung MC, Teng YC, Tsai TF, Chi YH. Progerin in muscle leads to thermogenic and metabolic defects via impaired calcium homeostasis. Aging Cell. 2020; 19:e13090. https://doi.org/10.1111/acel.13090 PMID:31833196

34. Lopez-Mejia IC, de Toledo M, Chavey C, Lapasset L, Cavelier P, Lopez-Herrera C, Chebli K, Fort P, Beranger G, Fajas L, Amri EZ, Casas F, Tazi J. Antagonistic functions of LMNA isoforms in energy expenditure and lifespan. EMBO Rep. 2014; 15:529–39. https://doi.org/10.1002/embr.201338126 PMID:24639560

35. López-Otín C, Galluzzi L, Freije JM, Madeo F, Kroemer G. Metabolic control of longevity. Cell. 2016; 166:802–21. https://doi.org/10.1016/j.cell.2016.07.031 PMID:27518560

36. Ducker GS, Rabinowitz JD. One-carbon metabolism in health and disease. Cell Metab. 2017; 25:27–42. https://doi.org/10.1016/j.cmet.2016.08.009 PMID:27641100

37. Chamberlin ME, Ubagai T, Mudd SH, Thomas J, Pao VY, Nguyen TK, Levy HL, Greene C, Freehauf C, Chou JY. Methionine adenosyltransferase I/III deficiency: novel mutations and clinical variations. Am J Hum Genet. 2000; 66:347–55. https://doi.org/10.1086/302752 PMID:10677294

38. Bárcena C, Quirós PM, Durand S, Mayoral P, Rodríguez F, Caravia XM, Mariño G, Garabaya C, Fernández-García MT, Kroemer G, Freije JM, López-Otín C. Methionine restriction extends lifespan in progeroid mice and alters lipid and bile acid metabolism. Cell Rep. 2018; 24:2392–403. https://doi.org/10.1016/j.celrep.2018.07.089 PMID:30157432

39. Hasty P, Sharp ZD, Curiel TJ, Campisi J. mTORC1 and p53: clash of the gods? Cell Cycle. 2013; 12:20–25. https://doi.org/10.4161/cc.22912 PMID:23255104

40. Hansen M, Rubinsztein DC, Walker DW. Autophagy as a promoter of longevity: insights from model organisms. Nat Rev Mol Cell Biol. 2018; 19:579–93. https://doi.org/10.1038/s41580-018-0033-y PMID:30006559

41. Schneider JL, Cuervo AM. Autophagy and human disease: emerging themes. Curr Opin Genet Dev. 2014; 26:16–23. https://doi.org/10.1016/j.gde.2014.04.003 PMID:24907664

42. Madrigal-Matute J, Cuervo AM. Regulation of liver metabolism by autophagy. Gastroenterology. 2016; 150:328–39. https://doi.org/10.1053/j.gastro.2015.09.042 PMID:26453774

43. Mariño G, Ugalde AP, Salvador-Montoliu N, Varela I, Quirós PM, Cadiñanos J, van der Pluijm I, Freije JM, López-Otín C. Premature aging in mice activates a systemic metabolic response involving autophagy induction. Hum Mol Genet. 2008; 17:2196–211. https://doi.org/10.1093/hmg/ddn120 PMID:18443001

44. Mariño G, López-Otín C. Autophagy and aging: new lessons from progeroid mice. Autophagy. 2008; 4:807–09. https://doi.org/10.4161/auto.6478 PMID:18612261

45. Vilchez D, Saez I, Dillin A. The role of protein clearance mechanisms in organismal ageing and age-related diseases. Nat Commun. 2014; 5:5659. https://doi.org/10.1038/ncomms6659 PMID:25482515

46. van Deursen JM. The role of senescent cells in ageing. Nature. 2014; 509:439–46. https://doi.org/10.1038/nature13193 PMID:24848057

47. Takeda T, Hosokawa M, Takeshita S, Irino M, Higuchi K, Matsushita T, Tomita Y, Yasuhira K, Hamamoto H, Shimizu K, Ishii M, Yamamuro T. A new murine model of accelerated senescence. Mech Ageing Dev. 1981; 17:183–94. https://doi.org/10.1016/0047-6374(81)90084-1 PMID:7311623

48. Riera-Borrull M, Rodríguez-Gallego E, Hernández-Aguilera A, Luciano F, Ras R, Cuyàs E, Camps J, Segura-Carretero A, Menendez JA, Joven J, Fernández-Arroyo S. Exploring the process of energy generation in pathophysiology by targeted metabolomics: performance of a simple and quantitative method. J Am Soc Mass Spectrom. 2016; 27:168–77. https://doi.org/10.1007/s13361-015-1262-3 PMID:26383735

49. Rossella F, Polledri E, Bollati V, Baccarelli A, Fustinoni S. Development and validation of a gas chromatography/mass spectrometry method for the assessment of genomic DNA methylation. Rapid Commun Mass Spectrom. 2009; 23:2637–46. https://doi.org/10.1002/rcm.4166 PMID:19630031

50. Chong J, Soufan O, Li C, Caraus I, Li S, Bourque G, Wishart DS, Xia J. MetaboAnalyst 4.0: towards more transparent and integrative metabolomics analysis. Nucleic Acids Res. 2018; 46:W486–94. https://doi.org/10.1093/nar/gky310 PMID:29762782
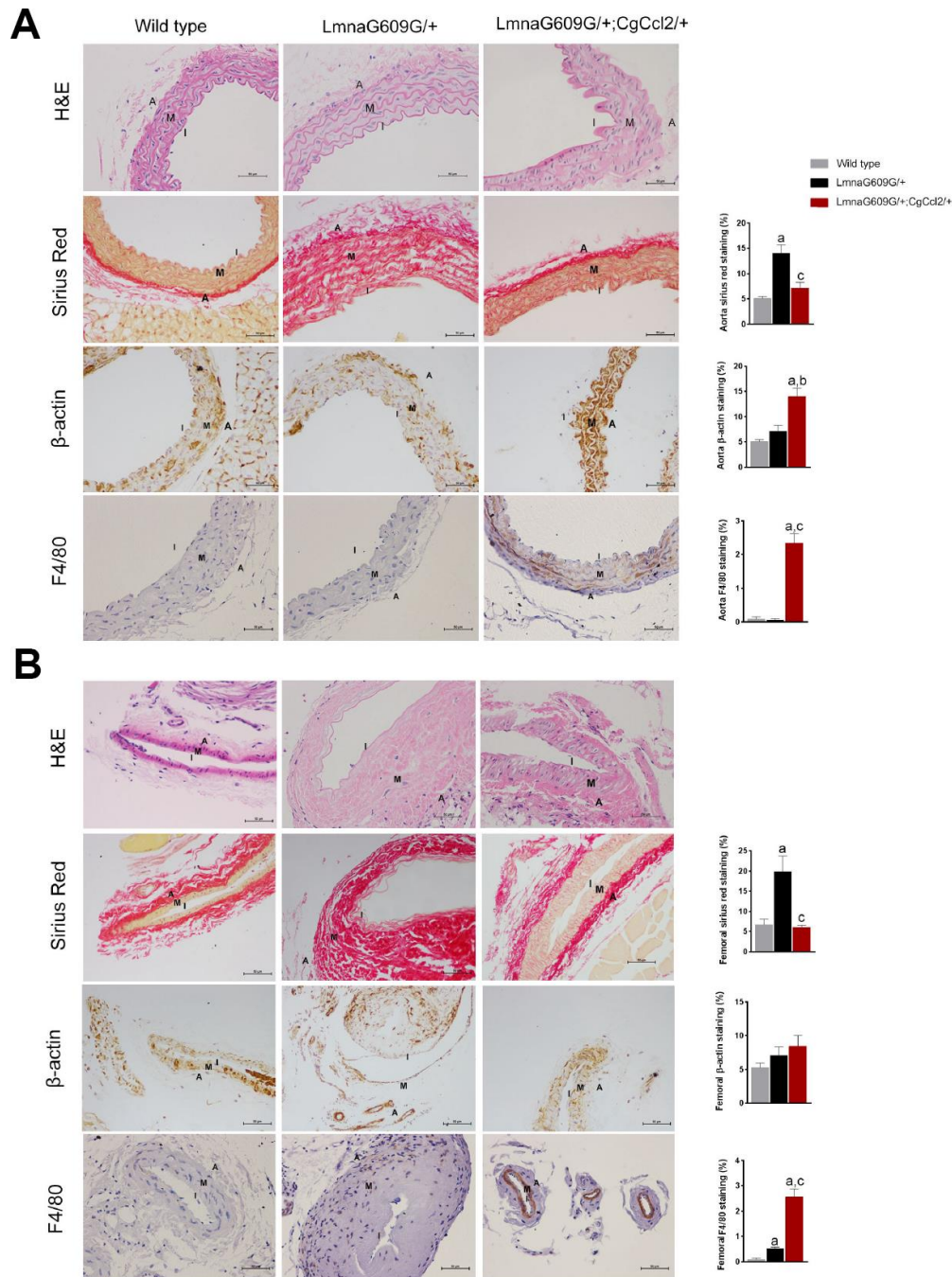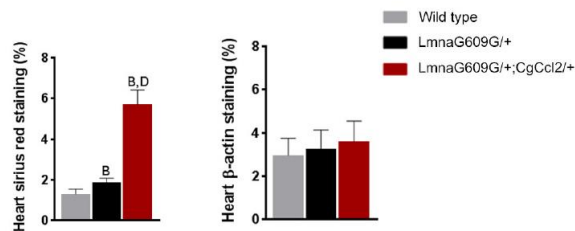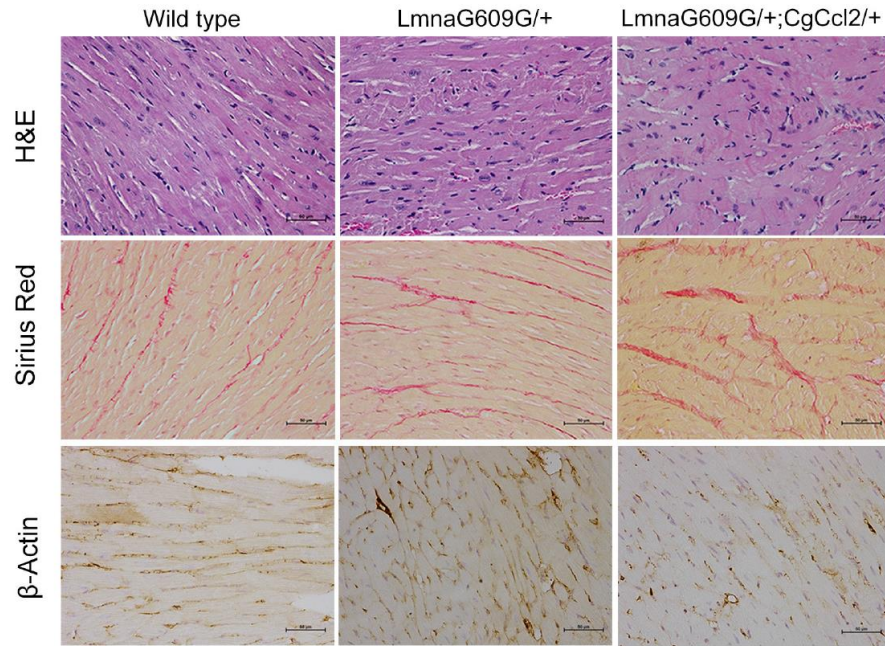
Supplementary Figure 1. Histological alterations in major arteries were accelerated by Ccl2 overexpression. The structure and composition of the aorta (**A**) and femoral arteries (**B**) were clearly disturbed in the progeroid mice with respect to the controls, and Ccl2 exacerbated this negative impact. Representative micrographs taken after staining with hematoxylin and eosin (H&E) and Sirius red and the immunohistochemical analysis of β-actin and F4/80 cells are shown. Results from the measurements of positively stained areas are shown as the means ± SEM. Statistical comparisons of the LMNAG609G/+;Cg CCL2/+ mice are depicted as a p<0.001 with respect to the wildtype mice, b p<0.05 with respect to the LMNAG609G/+ mice and c p<0.001 with respect to the LMNAG609G/+ mice according to the Mann–Whitney U test (n=5 for each strain). LMNAG609G/+ ; Cg CCL2/+ and LMNAG609G/+ denote progeroid mice with and without Ccl2 overexpression, respectively.

Supplementary Figure 2. Alterations in the histological structure of cardiac muscles of the progeroid mice. (**A**) Representative photograph of animal hearts. (**B**) Representative micrographs of heart sections stained with hematoxylin and eosin (H&E) and Sirius red and results from the immunohistochemical analysis of β-actin showing structural changes, with increased fibrosis being the only feature significantly affected by Ccl2 overexpression. Results from measurements of the positively stained areas are shown as the means ± SEM. Statistical comparisons with the LMNAG609G/+;CGCCL2+/- mice are depicted as a p<0.05 with respect to the wild-type mice and b p<0.05 with respect to the LMNAG609G/+ mice according to the Mann−Whitney U test (n=5 for each strain). LMNAG609G/+;Cg CCL2/+ and LMNAG609G/+ denote progeroid mice with and without Ccl2 overexpression, respectively.
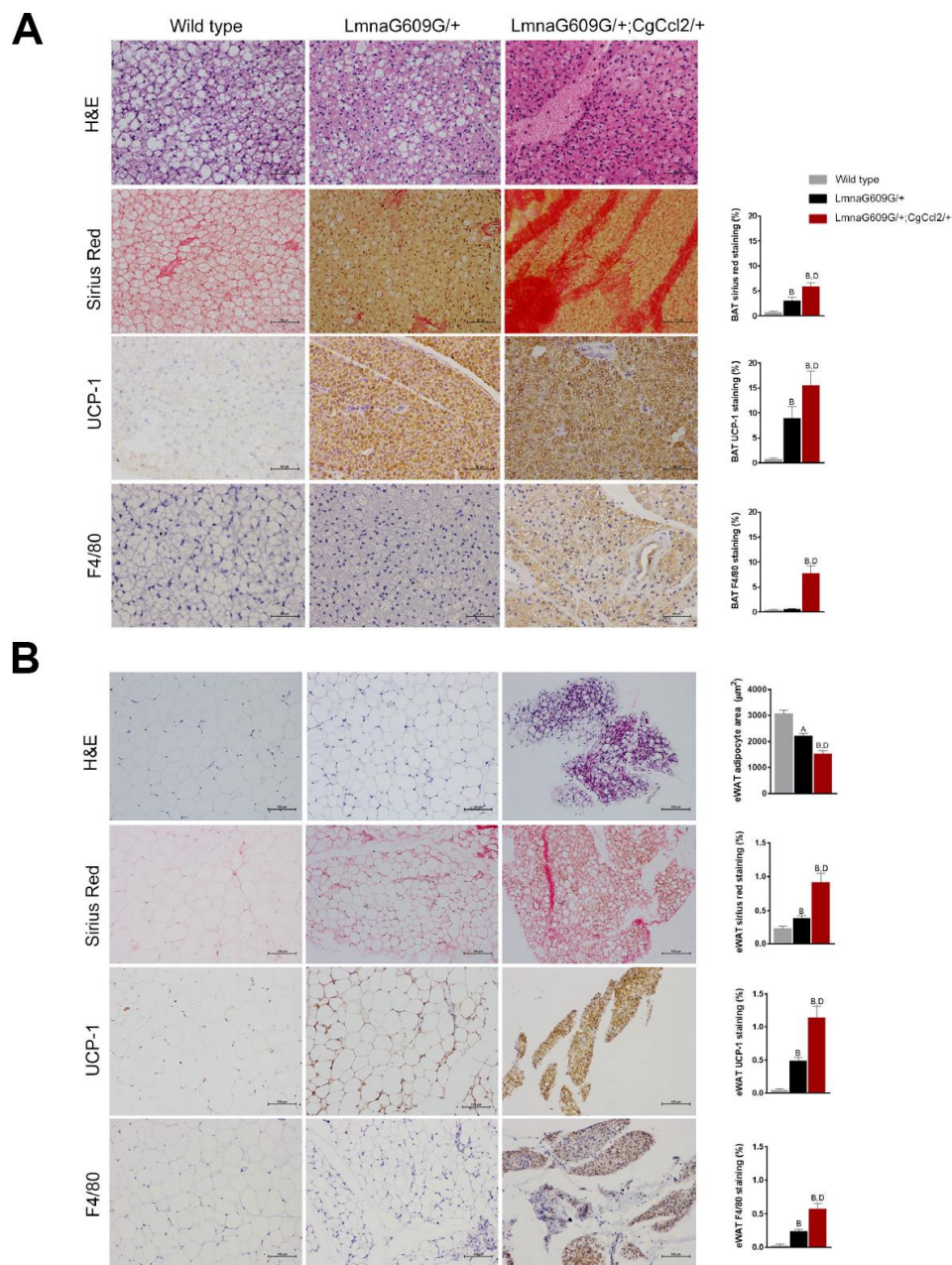
Supplementary Figure 3. The generalized loss of fat depots in the progeroid mice was augmented in the mice with Ccl2 overexpression. Representative micrographs of (**A**) brown (BAT) and (**B**) epididymal white adipose tissue (eWAT) stained with hematoxylin and eosin (H&E) and Sirius red and the results of the immunohistochemical analysis of uncoupling protein one (UCP-1) and F4/80 cells, showing structural changes and the negative impact of Ccl2 overexpression. Results from the measurements of positively stained areas are shown as the means ± SEM. Statistical comparisons with the LMNAG609G/+;Cg CCL2/+ mice are depicted as a p<0.05 with respect to the wild-type mice and b p<0.05 with respect to the LMNAG609G/+ mice according to the Mann−Whitney U test (n=5 for each strain). LMNAG609G/+;Cg CCL2/+ and LMNAG609G/+ denote progeroid mice with and without Ccl2 overexpression, respectively.
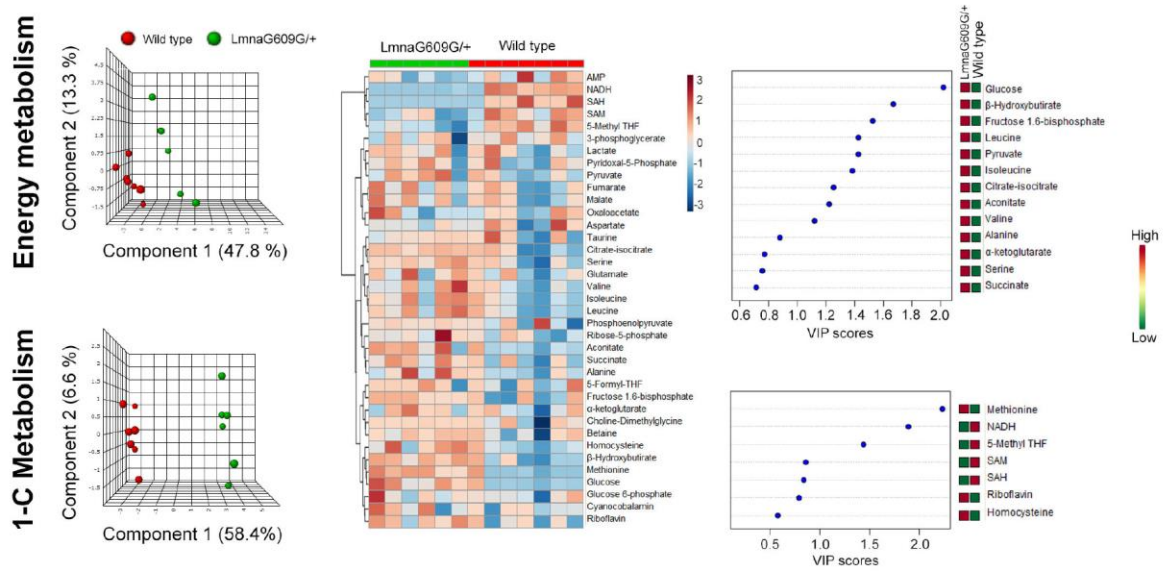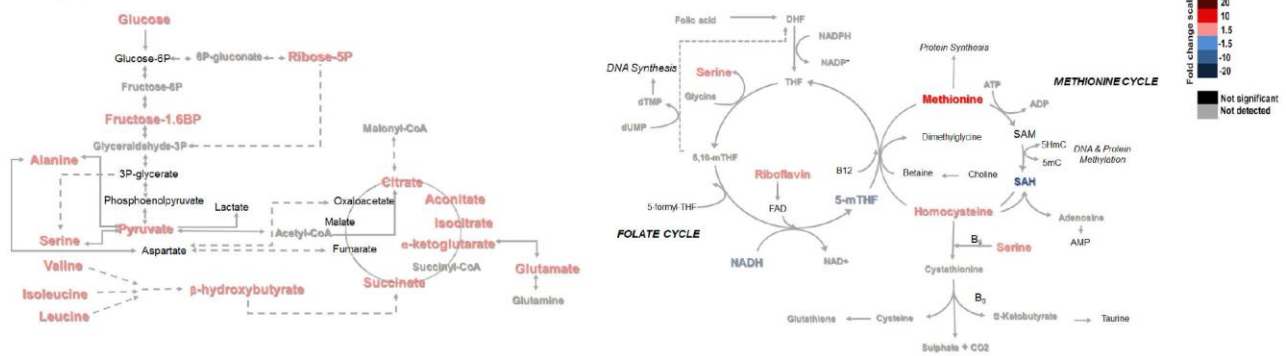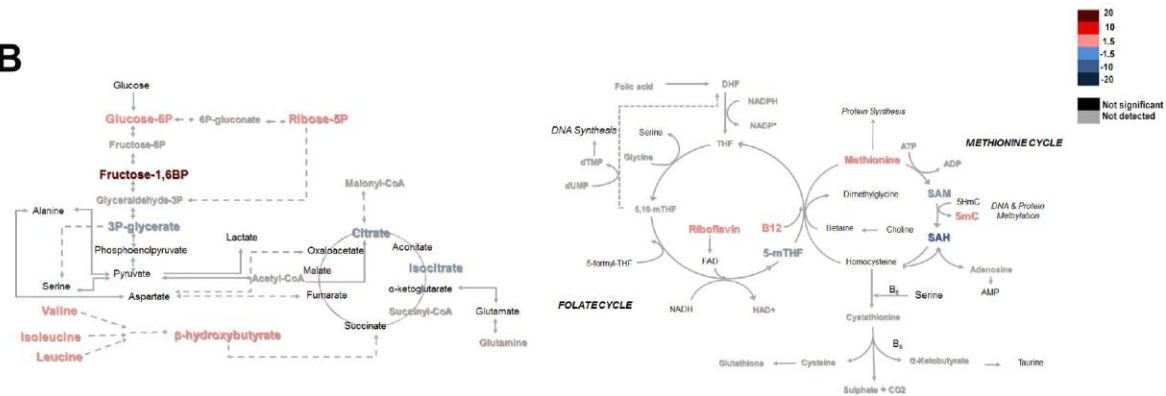
Supplementary Figure 4. Metabolomic analysis of skeletal muscle from LMNAG609G/+ mice and the control group. (**A**) From left to right, partial least square discriminant analysis (PLSDA), heatmap with hierarchical clustering and random forest analysis indicating that Lamin A mutation drove the changes in energy and one-carbon metabolism in the samples from quadriceps muscles. The levels of metabolites distinguish the muscles from this strain from the muscles of the controls (n = 8). The variables of the highest importance, according to the projection scores, were glucose and methionine. (**B**) Comparison of the levels of metabolite abundance from glycolysis and the citric aid cycle in the quadriceps muscles. The relative impact of the Lmna mutation (LMNAG609G/+) was assessed by fold changes, and indicated in the legend, and suggested a failed attempt to increase energy expenditure and attenuate the dysregulation of the methionine cycle.
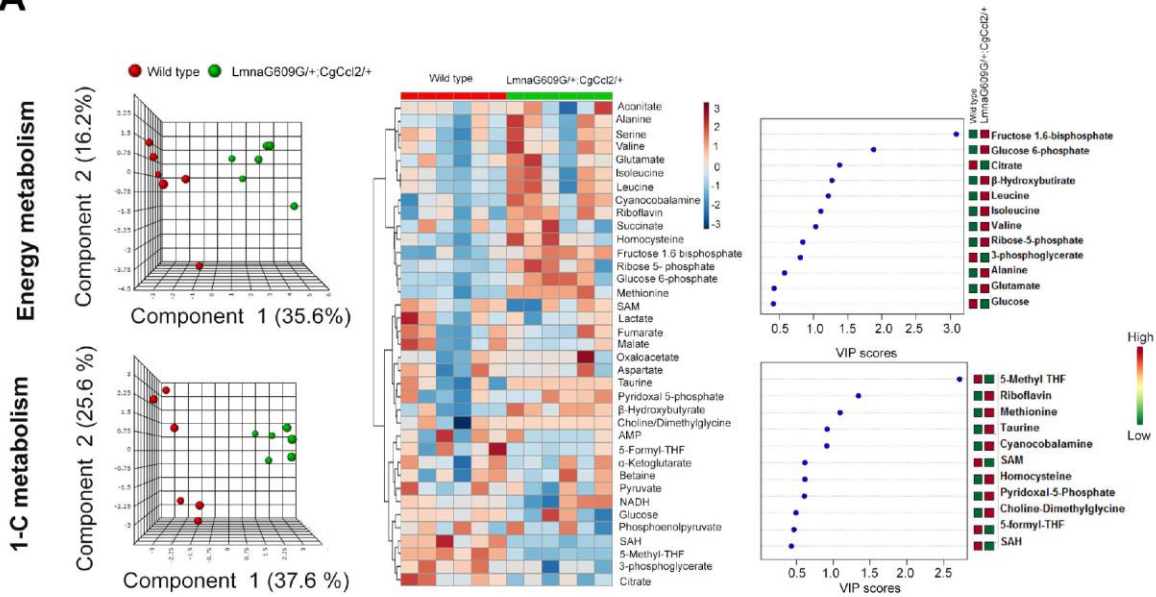
Supplementary Figure 5. Metabolomic analysis of skeletal muscle from LMNAG609G/+;Cg CCL2/+ mice and the control group. (**A**) From left to right, partial least square discriminant analysis (PLSDA), heatmap with hierarchical clustering and random forest analysis indicating that Ccl2 overexpression contributed to the metabolic defects observed in the mice with the simple Lamin A mutation. Consequently, changes in the metabolites of energy and one-carbon metabolism in the samples from quadriceps muscles distinguished the muscles of this strain from the muscles of controls (n = 8). The variables of highest importance, according to the projection scores, were fructose 1,6 biphosphate and 5-methyl tetrahydrofolate (**B**). The relative impact of the LMNAG609G/+;Cg CCL2/+ mutation on the levels of metabolites associated with energy and one-carbon metabolism was assessed by fold changes, as indicated in the legend. The results suggest major defects in the pentose phosphate pathway and folate cycle.
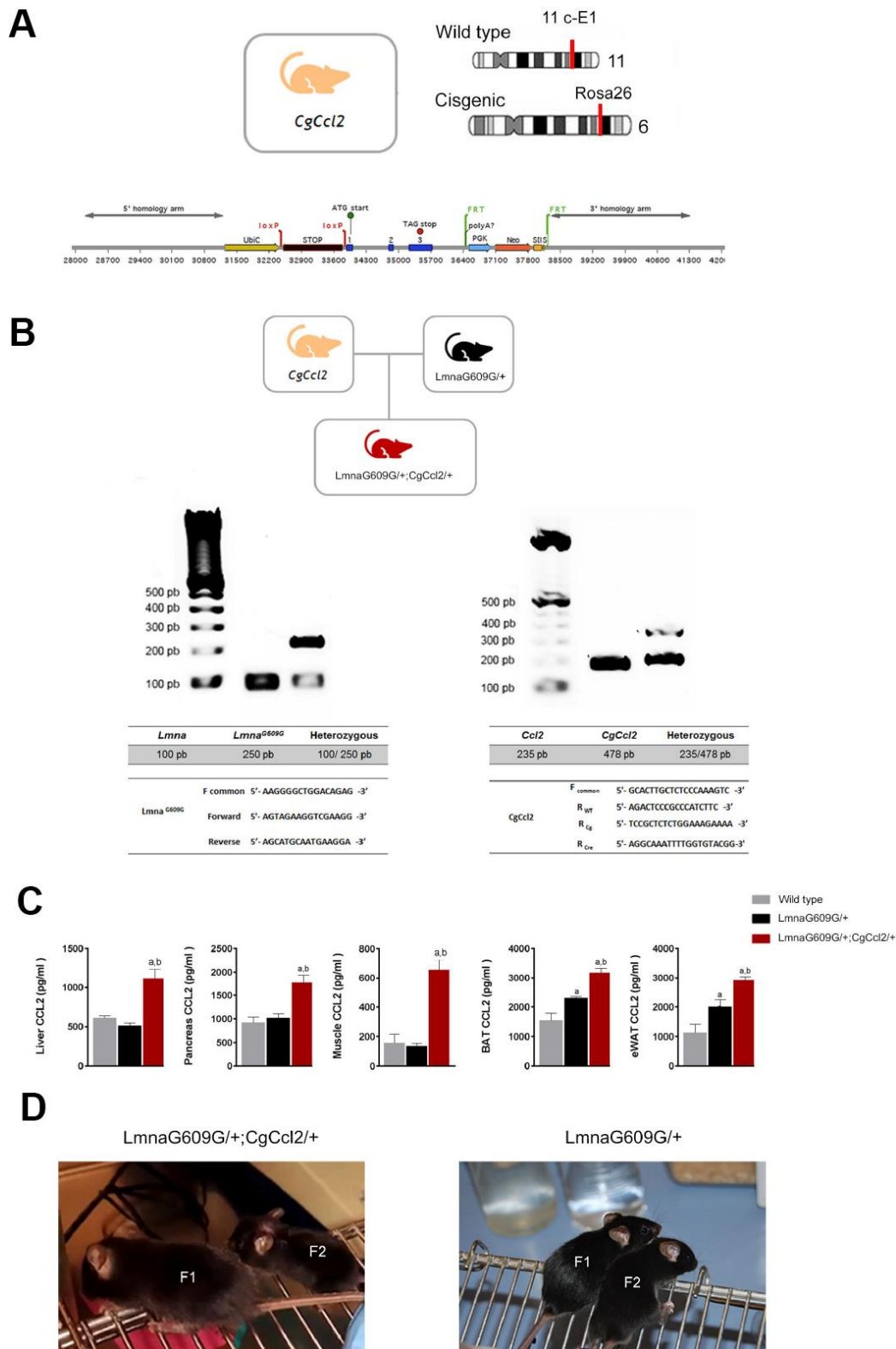
Supplementary Figure 6. Experimental models. (**A**) An additional copy of the C-C motif ligand 2 gene (Ccl2) was inserted via recombination into embryonic stem cells at the ROSA26 locus of chromosome 6 to overexpress Ccl2 [20]. (**B**) Offspring from crossbreeding were systematically genotyped using the described primers to identify the progeroid mice with (LMNAG609G/+;Cg CCL2/+ and without (LMNAG609G/+) [23] Ccl2 overexpression. (**C**) Tissue extracts were used to measure Ccl2 concentration. Results are expressed as the means ± SEM (n = 8-12). Mann−Whitney U tests revealed significant differences denoted as ap< 0.05 with respect to the wild-type mice and bp<0.05 with respect to the LMNAG609G/+ mice. (**D**) F2 littermates of the LMNAG609G/+;Cg CCL2/+ mice were of lower weight and not fertile.

Supplementary Tables

Supplementary Table 1. Energy-balance metabolites in skeletal muscle. Values were expressed in µM/100 mg of tissue (mean and interquartile range).

Metabolites	Wild type	LMNAG609G/+	LMNAG609G/+;Cg CCL2/+
Glucose	373.4 (345-394.2)	1101 (819.4-2248.1)[a]	175.6 (104.5-517.3)[c]
Glucose 6-phosphate	16 (12.8-18.8)	18.2 (14.1-19.7)	131.3 (77.4-166.3)[a,c]
Fructose-1.6-Bisphosphate	3.6 (2.4-13.4)	12.4 (12.4-19.9)[a]	87.9 (55.5-120.4)[a,c]
3-phosphoglycerate	1.9 (1.6-3.2)	1.3 (0.4-2.6)	1.4 (0.8-1.5)[a,c]
Phosphoenolpyruvate	0.5 (0.3-1.1)	0.7 (0.7-0.8)	0.3 (0.1-1.6)[c]
Pyruvate	68.8 (54.8-221.2)	475.6 (248.2-482.6)[a]	107.1 (40-142.4)[c]
Lactate	9815.7 (6626.5-16649.8)	12913.7 (4688.9-16340.4)	9730.5 (8019.7-10986.5)
Ribose-5-phosphate	9 (7.8-9)	10.4 (10.2 -10.7)[a]	20.9 (20.3-29.2)[a,c]
Oxaloacetate	27.7 (15.7-33.4)	19.8 (19.8-38.5)	29.2 (20.7-29.2)
Citrate-isocitrate	51.6 (27.1-119.4)	137.5 (137.5-137.5)[a]	22.8 (11.5-31)[a,d]
Aconitate	11.5 (10.3-12.9)	32.6 (29.4-34.6)[a]	12.7 (7.9-29.4)[c]
α-ketoglutarate	2.1 (1.2-5.1)	3.7 (1.2-5.2)[a]	1.6 (1.2-5.2)
Succinate	41.2 (38.1-79.1)	71.1 (66.5-104.5)[a]	47.8 (25.4-83.5)
Fumarate	143.7 (56.9-217.6)	337.4 (229.7-337.4)	131.9 (89.1-160.5)[c]
Malate	322.2 (133.8-502)	593 (387.8-704.6)	231 (203.7-326.1)[c]
β-Hydroxybutirate	38.4 (22-51.3)	129.9 (97.6-147.4)[a]	99.5 (82.9-111.9)[a]
Glutamate	1673 (1212.6-2498.8)	2798.1 (1842.4-3290.2)[a]	2058.4 (1558.2-3866.8)
Alanine	362.2 (286.4-414.6)	619.2 (396.8-1193.4)[a]	489.4 (342.4-855.5)
Serine	1007.8 (591.2-1375)	1585.4 (1360-2012.6)[a]	1309.3 (956.5-1466)
Valine	123.3 (75.9-201.2)	357.5 (164-814.4)[a]	258 (220.7-507.8)[a]
Isoleucine	77.1 (45-116.7)	317.9 (126.3-341.8)[a]	174.6 (101.1-438.8)[a]
Leucine	163.8 (102-260.6)	612.9 (287-851.5)[a]	416 (267.4-1153.4)[a]
Aspartate	245 (108.4-374.3)	195.5 (195.5-201.5)	206.3 (139-219.3)

[a] p < 0.05, [b] p< 0.001, with respect to wild type; [c] p<0.05, [d] p<0.001, with respect to LMNAG609G/+ by Mann–Whitney U test. *LMNAG609G/+*;Cg CCL2/+ *andLMNAG609G*/+ denote progeroid mice with and without Ccl2, respectively.

Supplementary Table 2. Metabolites from one-carbon metabolism in skeletal muscle.

Metabolites	Wild type	LMNAG609G/+	LMNAG609G/+;CgCCL2/+
Taurine	1499.7 (601.8-3621.9	1952.7 (1407-2041.3)	3038.1 (2920.8-3038.1)[d]
Choline-Dimethylglycine*	145.9 (69.1-216.1)	185.7 (185.7-189.4)	171.6 (171.0-171.8)[d]
Betaine*	0.4 (0.2-0.5)	0.6 (0.5-0.6)	0.3 (0.3-0.6)
Homocysteine	0.3 (0.3-0.4)	0.7 (0.5-0.9)[a]	0.5 (0.3-0.9)
SAM	3.3 (1.7-4.5)	1.2 (0.7-2.0)	2.7 (0.5-2.1)[a,c]
Methionine	0.6 (0.6-0.7)	9.3 (6.4-12.2)[a]	1.6 (0.8-1.6)[a,d]
AMP	3.7 (2.1-5.7)	2.3 (1.5-2.9)	2.8 (2.8-3.8)[c]
NADH	1.7 (1.3-2.5)	0.2 (0.2-0.2)[a]	5 (0.2-3.8)[d]
SAH*	0.1 (0.1-0.2)	0.01 (0.0-0.01)[a]	0.09 (0.07-0.1)[b,d]
Pyridoxal 5 phosphate	3.5 (2.2-7.1)	4.9 (4.4-6.4)	6.7 (4.1-9.6)
5-Methyl-THF*	10.2 (8.8-20.1)	3.2 (1.2-3.2)[a]	1.1 (0.9-1.3)[a,c]
5-Formyl-THF*	1.7 (0.7-2.8)	2.1 (2.1-2.1)	0.8 (0.8-1.3)[c]
Cyanocobalamin*	0.4 (0.3-0.5)	0.5 (0.4-0.8)	0.8 (0.5-1)[a]
Riboflavin	0.5 (0.2-0.9)	1.2 (0.9-1.7)[b]	1.7 (0.9-2.2)[a]

Values were expressed in µM/ 100 mg of tissue (mean and interquartile range) or * nM/100 mg of tissue. [a] $p < 0.05$, [b] $p < 0.001$, with respect to wild type; [c] $p<0.05$, [d] $p<0.001$, with respect to LMNAG609G/+ by Mann–Whitney U test. LMNAG609G/+;*CgCCL2/+* and LMNAG609G/+ denote progeroid mice with and without *Ccl2*, respectively. SAM: s-adenosylmethionine; AMP: Adenosine monophosphate; SAH: s-adenosylhomocysteine; 5-Methyl-THF: 5-Methyl-tetrahydrofolate; 5-Formyl-THF: 5-Formyl-tetrahydrofolate.

Supplementary Table 3. Criteria for grading score of senescence in mice.

	Grade 0	Grade 1	Grade 2	Grade 3	Grade 4
Behavior					
Reactivity	The most intensive exploratory response observed within 30 seconds	Normal behavior	Abnormal grait with no lessening of agility and behavior patterns and restlessness	Definite decrease in agility and behavior patterns	Does not move voluntarily but will move if nudged	Immobile
Passivity	Escape reaction from pinching of the nuchal skin or from hanging by the forelimb	Natural escape reaction to pinching	Decrease in escape reaction to pinching	Loss of escape reaction to pinching. Preserved righting reaction to manual turn over	Neither escape reaction to pinching nor righting to hanging by the forelimb.	Escape reaction nil
Appearance					
Glossiness	Glossiness	Natural gloss	Decrease in gloss	Complete disappearance of gloss	Complete disappearance of gloss and hair appears dirty	Complete disappearance of gloss and hair looks very dirty
Coarseness	Coarseness of hair on the head, nuca and dorsum determined according to the number of palpable, fine clumps of hair	No coarseness	Coarseness of less than an area of the head	Coarseness of less than double the area of the head	Coarseness of less than 3 times area of the head	Coarseness of over 3 times area of the head
Loss of hair	Loss or thinning of hair on the head, nuca and dorsum except for changes due to ulcer or Periophthalmic lesions	Neither loss or thinning of hair	A. Loss of hair in less than an area of the head. B. Thinning of hair in less than 1/2 of total area	A. Loss of hair in over one area of the head, less than in 1/4 of total area. B. Thinning if hair in more than 1/2 of total area	Loss of hair in more than 1/4, in less than 1/2 of total area.	Loss of hair in over 1/2 of total area
Skin ulcers	Ulcer or healed ulcer on entire skin except for changes associated with Periophthalmic lesions	No evidence of ulcer	Healed ulcer or ulcer with scab	Ulcer without healing tendency, in less than one area of the head	Ulcer without healing tendency in more than one area of the heard, in less than 1/4 area of all the skin.	Ulcer without healing tendency in more than 1/4 area of whole skin
Eyes					
Periophthalmic lesions	Catarrhal changes in the periophthalmic area or swelling of the palpebra	No changes	Catarrhal changes limited to periophthalmic area or swelling of palpebra	Catarrhal changes extending to nose	Catarrhal changes extending further	
Lordokyphosis of the spine	Examined by inspection and palpation	Natural anteroposterior curvature	Increased curvature disappears with digital pressure on the dorsum	Increased curvature disappears with a combination of manual cephalocaudal traction and digital pressure on the dorsum	permanent curvature	Lordokyphosis of the spine

Supplementary Table 4. Antibodies used in western blot and immunohistochemical analyses.

Antigen	Antibody	1ry Dilution	2ry Antibody	2ry Dilution
CD11b	CD11b antibody, ab133357 (Abcam, Cambridge, UK)	1:1000	Goat α-rabbit HRP, P0448 (Dako, Santa Clara, CA, USA)	1:5000
TNFα	TNFα antibody, #3707 (Cell signalling, Danvers, MA, USA)	1:1000	Goat α-rabbit HRP, P0448 (Dako, Santa Clara, CA, USA)	1:5000
CD163	CD163, antibody, ab182422 (Abcam, Cambridge, UK)	1:1000	Goat α-rabbit HRP, P0448 (Dako, Santa Clara, CA, USA)	1:5000
F4/80	F4/80, antibody, ab100790 (Abcam, Cambridge, UK)	1:100	Goat α-rabbit HRP, P0448 (Dako, Santa Clara, CA, USA)	1:200
Arginase	Liver arginase, antibody, ab91279 (Abcam, Cambridge, UK)	1:10000	Goat α-rabbit HRP, P0448 (Dako, Santa Clara, CA, USA)	1:5000
PON1	In-house	1:200	Goat α-rabbit HRP, P0448 (Dako, Santa Clara, CA, USA)	1:1000
PI3K-p85	PI3K antibody, #4257 (Cell signalling, Danvers, MA, USA)	1:1000	Goat α-rabbit HRP, P0448 (Dako, Santa Clara, CA, USA)	1:5000
Akt pS473	p-Akt antibody, #4060 (Cell signalling, Danvers, MA, USA)	1:1000	Goat α-rabbit HRP, P0448 (Dako, Santa Clara, CA, USA)	1:5000
Akt	AKT antibody, #4685 (Cell signalling, Danvers, MA, USA)	1:1000	Goat α-rabbit HRP, P0448 (Dako, Santa Clara, CA, USA)	1:5000
S6 pS235/236	p-pS6 antibody, #4856 (Cell signalling, Danvers, MA, USA)	1:1000	Goat α-rabbit HRP, P0448 (Dako, Santa Clara, CA, USA)	1:5000
S6	S6 antibody, #2217 (Cell signalling, Danvers, MA, USA)	1:1000	Goat α-rabbit HRP, P0448 (Dako, Santa Clara, CA, USA)	1:5000
P53 p-S15	P-P53 antibody, #9284 (Cell signalling, Danvers, MA, USA)	1:1000	Goat α-rabbit HRP, P0448 (Dako, Santa Clara, CA, USA)	1:500
P53	P53 antibody, #2524 (Cell signalling, Danvers, MA, USA)	1:1000	Goat α-mouse HRP, P0447 (Dako, Santa Clara, CA, USA)	1:500
AMPK pT172	p-AMPK antibody, #2531 (Cell signalling, Danvers, MA, USA)	1:1000	Goat α-rabbit HRP, P0448 (Dako, Santa Clara, CA, USA)	1:5000
AMPK	AMPK antibody #2532S (Cell signalling, Danvers, MA, USA)	1:1000	Goat α-rabbit HRP, P0448 (Dako, Santa Clara, CA, USA)	1:5000
OXPHOS	OXPHOS Rodent,antibody, ab ab110413 (Abcam, Cambridge, UK)	1:250	Goat α-mouse HRP, P0447 (Dako, Santa Clara, CA, USA)	1:5000
LC3	LC3B Antibody, #2775S (Cell signalling, Danvers, MA, USA)	1:1000	Goat α-rabbit HRP, P0448 (Dako, Santa Clara, CA, USA)	1:5000
LAMP2A	LAMP2A antibody, ab125068 (Abcam, Cambridge, UK)	1:1000	Goat α-rabbit HRP, P0448 (Dako, Santa Clara, CA, USA)	1:2000
P62	P62 Antibody, #5114 (Cell signalling, Danvers, MA, USA)	1:1000	Goat α-rabbit HRP, P0448 (Dako, Santa Clara, CA, USA)	1:5000
Vinculin	Vinculin antibody, ab73412 (Abcam, Cambridge, UK)	1:1000	Goat α-rabbit HRP, P0448 (Dako, Santa Clara, CA, USA)	1:2000
TOM20	TOM20 antibody, #42406 (Cell signalling, Danvers, MA, USA)	1:1000	Goat α-rabbit HRP, P0448 (Dako, Santa Clara, CA, USA)	1:5000
Mfn2	Mfn2 antibody, ab124773 (Abcam, Cambridge, UK)	1:1000	Goat α-rabbit HRP, P0448 (Dako, Santa Clara, CA, USA)	1:2000
UCP-1	UCP-1, antibody, ab10983(Abcam, Cambridge, UK)	1:100	Goat α-rabbit HRP, P0448 (Dako, Santa Clara, CA, USA)	1:200